Magnonic Domain Wall Heat Conductance in Ferromagnetic Wires

Peng Yan[1] and Gerrit E. W. Bauer[2,1]

[1]Kavli Institute of NanoScience, Delft University of Technology, Lorentzweg 1, 2628 CJ Delft, Netherlands
[2]Institute for Materials Research, Tohoku University, Sendai 980-8577, Japan

(Received 18 April 2012; published 21 August 2012)

We present a theoretical study of magnon-mediated heat transport in electrically insulating ferromagnetic wires containing a domain wall (DW). In the regime of validity of continuum micromagnetism, a DW is found to have no effect on the heat conductance. However, spin waves are found to be reflected by DWs with widths of a few lattice spacings, which is associated with emergence of an additional spin wave bound state. The resulting DW heat conductance should be significant for thin films of yttrium iron garnet with sharply defined magnetic domains.

DOI: 10.1103/PhysRevLett.109.087202 PACS numbers: 75.30.Ds, 75.60.Ch, 85.75.−d

Spin wave (SW) excitations in magnetic systems have been studied for many decades, but due to recent progress in the fabrication of magnetic nanostructures, novel detection techniques, and new discoveries such as current-induced magnetization dynamics, the field is very much alive [1]. SWs can be used to transmit information and probe magnetic properties. SW logic device concepts have been proposed [2,3]. Recent experiments show that three crucial material parameters, namely, the spin polarization P, the Gilbert damping α, and the dissipative correction to adiabaticity β, can be simultaneously determined by measuring the current-induced SW Doppler effect [4,5]. Nonvolatile data storage devices [6] and logic circuits [7] make use of magnetic domain walls (DWs). The combination of both strategies is promising as well [8]. Phenomena based on the interaction between SWs and DWs have been found within the framework of continuum micromagnetic theory, such as absence of reflection of SWs by a DW [9] and associated scattering phase shifts [8,9], frequency doubling [10], DW drift [11–13], and magnonic spin-transfer torques [14–16]. A complication that has received much less attention is the breakdown of the continuum approximation of the magnetization in materials with high anisotropies, in which the DW width δ can be as small as a few lattice constants a [17]. Atomic-scale DWs can display very different static and dynamic properties than those predicted by a continuum model [18]. For example, discrete DW jumps that match the lattice periodicity have been observed by Novoselov *et al.* [19] in thin films of yttrium iron garnets (YIG) that support DWs as narrow as $\delta/a \approx 6/\pi$. Only one attempt to formulate the theory of SWs propagating through ultranarrow DWs is known to us [20], predicting that a SW can pass through a DW with little reflection if its wavelength is less than twice the thickness of the wall [20], which does not agree with our findings here.

In this Letter, we address DWs in wires of insulating ferromagnets such as YIG with damping constants that can be 3 orders of magnitude smaller than those in metallic magnets, which makes them attractive for novel magnetic device concepts. Charge current-induced DW motion is ruled out, of course, but heat currents can serve identical purposes by virtue of the thermal spin-transfer torque [15,21]. Here, we study SW excitations in ferromagnetically coupled spin chains in the presence of a DW, predicting significant effects of the discrete lattice on the SW transmission. While we confirm previous results that in a continuum model for DWs the SW transmission probability is unity, spin wave reflection in a discrete spin model is found to be finite for DWs with widths approaching the lattice parameter. The resulting DW heat conductance should help to detect and manipulate DWs in insulating ferromagnetic wires.

We consider a nanostructured wire or constriction that is sufficiently thin such that the lateral degrees of freedom are frozen out and a one-dimensional (1D) model is appropriate. Our model is a classical Heisenberg spin chain with local anisotropy and nearest-neighbor ferromagnetic exchange interaction, which is appropriate for materials such as YIG which has a large effective spin ($S \approx 14.3$) per unit cell [22]. In the Hamiltonian [23]

$$\mathcal{H} = -J\sum_{\langle n,m\rangle}\vec{S}_n\cdot\vec{S}_m - D\sum_n (S_n^z)^2, \tag{1}$$

the first term describes the nearest-neighbor interaction with ferromagnetic coupling $J > 0$, while the second term is a local easy-axis anisotropy in the z direction with $D > 0$. The local spin variable $\vec{S}_n$ is a three-component unit vector on the nth lattice site. Our approach developed below can be extended to thin films [24] with (in the absence of disorder) essentially the same physics, although a transverse hard axis (shape) anisotropy causes complicated spin wave dispersions. In our 1D system, the dipolar interaction can be important as well but only leads to an increased easy-axis anisotropy [23,25]. For materials with a large unit cell such as YIG, our approximation to integrate the magnetic moment distributions over the unit cell and replace them with one classical spin is a good approximation at low

temperatures (below 40 K) [26]. In insulating ferromagnets, the heat current is associated with both phonon and magnon channels. In YIG the magnons, responsible for interactions with DW of interest here, contribute 2/3 of the total heat current at low temperatures [27,28].

We consider a magnetic wire of length L that connects two large heat reservoirs held at two temperatures T_L, T_R, with constant difference $\Delta T = (T_L - T_R) > 0$. The magnon-mediated heat current carried by the spin chain is given by the Landauer-Büttiker formula [29]

$$\dot{Q} = \frac{1}{L}\int dk \rho_k v_k \hbar\omega_k |t_k|^2 [n_B(\omega_k, T_L) - n_B(\omega_k, T_R)] = \frac{1}{2\pi}\int d\omega \hbar\omega |t_{k(\omega)}|^2 [n_B(\omega, T_L) - n_B(\omega, T_R)]. \quad (2)$$

Here, $\rho_k = L/2\pi$ is the magnon density of states, $v_k = \partial\omega/\partial k$ is the SW group velocity, $\hbar\omega_k = 2D + 2J[1 - \cos(ka)]$ is the SW spectrum, t_k is the SW transmission coefficient, and $n_B(\omega, T_{L,R}) = 1/(e^{\hbar\omega/(k_B T_{L,R})} - 1)$ is the Bose–Einstein distribution. In the absence of DWs, $t_k = 1$ and for a small temperature bias

$$\dot{Q} = \frac{\Delta T}{2\pi}\int d\omega \hbar\omega \frac{\partial n_B(\omega, T)}{\partial T}, \quad (3)$$

where $T = (T_L + T_R)/2$.

The heat current in the presence of a DW depends on the magnetization profile, which is obtained by minimizing the energy with respect to the polar angle θ_n of $\vec{S}_n$ with the easy axis, which leads to

$$\sin(\theta_n - \theta_{n-1}) - \sin(\theta_{n+1} - \theta_n) + \frac{D}{J}\sin(2\theta_n) = 0, \quad (4)$$

where we chose the boundary conditions that spins are oriented in the $\pm z$ directions at the ends of the wire. The ground-state DW configuration can be computed iteratively [30]. To second order in the small parameter $D/J \ll 1$, this procedure yields the Walker solution $\text{lntan}(\theta/2) = z/\delta$ with DW width $\delta = a\sqrt{J/(2D)}$ [31]. In a typical (metastable) Walker DW, labeled A in Fig. 1, the spin of the central lattice site is oriented normal to the easy axis. However, numerical calculations find that type B walls (Fig. 1) have always lower energies [18]. Clearly, this difference is immaterial in the continuum limit for the magnetization (micromagnetics), but it is relevant for atomically sharp DWs. We will discuss below that the atomic-scale magnetization texture is observable in the heat and spin transport properties.

Proceeding from the ground-state DW configuration we can construct, linearize, and solve the equations of motion $d\vec{S}_n/dt = -\vec{S}_n \times (-\delta\mathcal{H}/\delta\vec{S}_n)$ for the spins at a site n in order to determine the frequencies and amplitudes of the allowed SW modes. This can be done conveniently in a coordinate system rotated about the x axis such that the transformed spins at equilibrium point to the new Z axis [32]. The spins in the two coordinate systems are related as

$$\begin{pmatrix} S_n^x \\ S_n^y \\ S_n^z \end{pmatrix} = \begin{pmatrix} 1 & 0 & 0 \\ 0 & \cos\theta_n & \sin\theta_n \\ 0 & -\sin\theta_n & \cos\theta_n \end{pmatrix} \begin{pmatrix} S_n^X \\ S_n^Y \\ S_n^Z \end{pmatrix}. \quad (5)$$

The low-energy excitations correspond now to a small-angle precession around the Z axis with $S_n^Z \sim 1$ [16,33]. The equations of motion for the SW amplitude at site n and frequency ω in the rotated frame read

$$-i\frac{\omega}{J}S_n^X = c_{n-1}S_{n-1}^Y + c_n S_{n+1}^Y - [c_{n-1} + c_n - \frac{2D}{J}(\sin^2\theta_n - \cos^2\theta_n)]S_n^Y,$$
$$-i\frac{\omega}{J}S_n^Y = -S_{n-1}^X - S_{n+1}^X + (c_{n-1} + c_n + \frac{2D}{J}\cos^2\theta_n)S_n^X, \quad (6)$$

where $c_n = \cos(\theta_n - \theta_{n+1})$. We obtain the eigenfrequencies ω and amplitudes S_n^X, S_n^Y numerically.

$D/J = 0.001$ leads to a broad DW profile [solid line in Fig. 2(a)] that cannot be distinguished from the Walker solution. The SW mode profile S_n^Y is also plotted (circles), with a frequency indicated in the plot. For a broad DW, the SW profile agrees very well with the analytical solution of the continuum model [dashed line in Fig. 2(a)], i.e., the Schrödinger equation [15].

$$\left[-\frac{d^2}{d\xi^2} + V(\xi)\right]\varphi(\xi) = q^2\varphi(\xi), \quad (7)$$

with $\xi = z/\delta$, $\varphi = S_X - iS_Y$, $q = k\delta$ with spin wave vector k. The scalar potential $V(\xi) = -2\text{sech}^2\xi$ originates from the noncommutativity of the local gauge transformation with the momentum operator [16], similar to electron transport in magnetic textures [34]. However, in contrast to electrons, the transformation does not generate a vector potential for the SWs. The solutions of Eq. (7) are a single bound state and a continuum of propagating SWs that are not reflected by the DW but pick up a wave number k-dependent phase shift $\eta(k) = 2\tan^{-1}\{1/(k\delta)\}$ [15] that

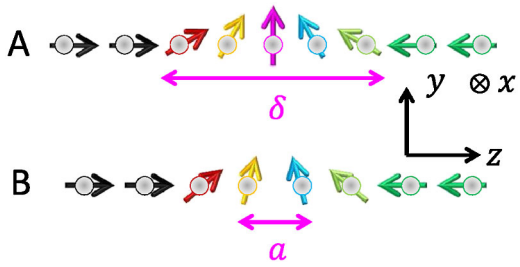

FIG. 1 (color online). Principle ground-state spin configurations for a symmetric DW: its center either coincides with one of the lattice sites (type A) or lies between them (type B). δ is the DW width, and a is the lattice constant.

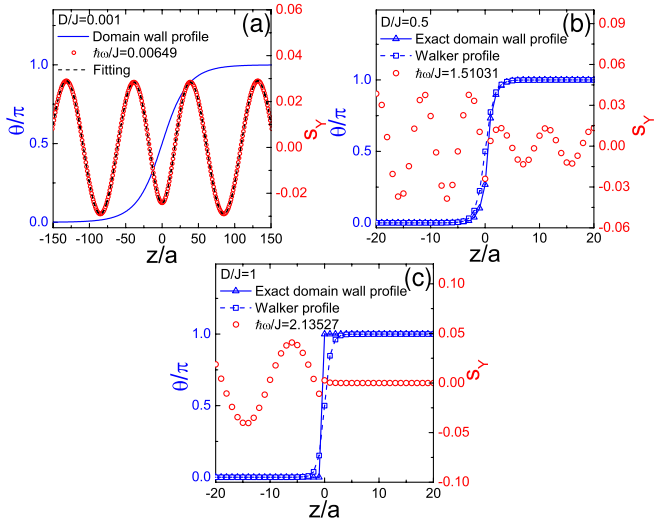

FIG. 2 (color online). (a) Magnetization profile of a wide head-to-head DW (solid line). The numerical SW solution (circles) for frequency ω in a linear ferromagnetic chain cannot be distinguished from the solution for the continuum model (dashed line). (b) A computed narrow DW profile (triangles) compared with the Walker model (squares). The SW amplitude for the indicated frequency is shown by circles. (c) The ground-state profile of an abrupt DW (triangles) compared with the Walker profile (squares). The SW amplitude for the indicated frequency is shown by circles.

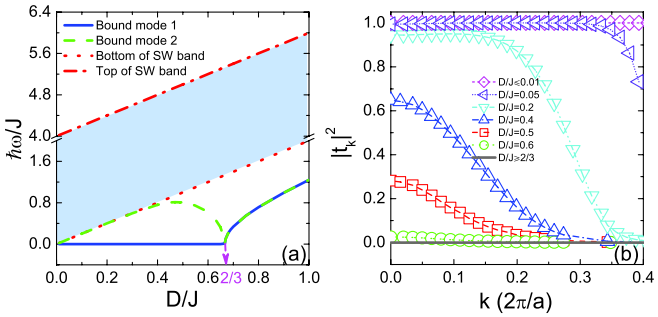

FIG. 3 (color online). (a) Frequencies of DW bound states and SW continuum (shaded area between dotted and dash-dotted lines). The solid curve represents the lowest mode, whereas the dashed curve shows the second bound state. (b) k dependence of SW transmission for different values of D/J.

modifies the frequency dispersion [35] and causes interference effects in rings [8]. Since the DW transmission coefficient is $t_k = e^{i\eta(k)}$ and the transmission probability is $|t_k|^2 = 1$, there is no DW limited heat transport. This conclusion is not modified by a transverse hard-axis anisotropy $D_\perp \sum_n (S_n^x)^2$, since propagating SWs are elliptical but still reflectionless. This conclusion holds despite the bound magnon state at the DW and in contrast to the results for conducting ferromagnets, where the bound state leads to an increase of the electric resistivity even in the continuum model [24]. In order to detect such a DW bound state in insulating ferromagnets, one has to resort to spectroscopic or other techniques [36].

The continuum approach breaks down for atomic scale DWs such as in Fig. 1. The profiles of a relatively narrow DW for both exact numerical (triangles) and Walker (squares) solution are shown in Fig. 2(b) for an anisotropy $D/J = 0.5$. We see that now spin waves do get reflected. Figure 2(c) shows the configuration of an abrupt DW (triangles) with $D/J = 1$. The Walker profile is also plotted for comparison (squares). Interestingly, we now find that all SWs (circles) are totally reflected. The physics is explained below.

As pointed out before, the DW supports bound SW states. Figure 3(a) shows the numerical results for the bound state frequencies as a function of D/J below the continuum SW region, where the dotted line delineates the SW gap ($\hbar\omega_g = 2D$) and the dash-dotted line indicates the top of the SW band ($\hbar\omega_t = 2D + 4J$). We confirm the existence of a transition point at $D/J = 2/3$ that separates smooth and sharp DW configurations [37] but without assuming $|\theta_{n\pm1} - \theta_n| \ll 1$, which is clearly not the case for these narrow DWs. The transition point obtained here differs from the value $D/J = 5/9$ calculated in Ref. [38]. Below the critical point, bound state 1 (solid curve) is caused by the axial symmetry of the Hamiltonian about the z axis. Bound state one can be interpreted as the symmetry restoring Goldstone mode in the presence of a domain wall with $\omega_{b1} = 0$. For wide DWs, i.e., $D/J \ll 2/3$, bound state 2 (dashed curve) merges with the continuum states. As the DW becomes narrower (increasing D/J), ω_{b2} splits from the SW continuum, which is due to the broken translational invariance of the DW when shrunk to the lattice scale, and displays a nonmonotonic dependence on D/J, with a maximum at $\hbar\omega_{b2} \approx 0.47D$ and dropping to zero when $D/J \to 2/3$. Above the critical point, the DW width coincides with the lattice constant and bound states 1 and 2 are degenerate, which can be traced to the disappearance of the DW chirality; the DW becomes axially symmetric and a zero frequency Goldstone mode cannot exist. By substituting an abruptly sharp DW profile into Eq. (6), we arrive directly at the conclusion that the wall completely reflect all SWs. We can also obtain the expression of the frequency of the degenerate bound states

$$\hbar\omega_{b1} = \hbar\omega_{b2} = J\sqrt{(24d^2 - 8d - 1 - \sqrt{16d^2 + 16d + 1})/6}$$

with $d = D/J$, which coincides with the numerical data. The critical value $D/J = 2/3$ is recovered for zero frequency.

We can now understand why the SW is reflected at ultranarrow DWs. Let us consider a confining potential $V(\xi) \to 0$ as $|\xi| \to \infty$ for which the eigenvalue problem Eq. (7) has N bound states with $q = i\kappa_n$, $n = 1, 2, \ldots, N$,

where κ_n is real. Through the inverse scattering formalism, one can construct a general $2N$-parameter formula for a reflectionless potential with N bound states [39],

$$V(\xi) = -2\frac{d^2}{d\xi^2} \ln \det A(\xi), \tag{8}$$

where the matrix $A_{mn}(\xi) = \delta_{mn} + \lambda_m\lambda_n/(\kappa_m + \kappa_n)$, with Kronecker function δ_{mn} and $\lambda_n(\xi) = f_n e^{-\kappa_n\xi}$, is symmetric. For $N = 1$, we recover the previous result of the continuum model [15]. In the discrete model, the inverse scattering formalism is still valid since the Schrödinger differential equation becomes a difference equation [40] with, however, $N = 2$. Figure 3(a) clearly shows that the bound state 2 vanishes into the SW continuum only for wide DWs ($D/J \ll 2/3$). Only in this limit, there is just one bound state (mode 1) and the DW profile is perfectly described by the reflectionless Walker model. To model the profile of a relatively narrow DW, we expand Eq. (4) to the fourth order and obtain the DW configuration $\ln\tan(\theta/2) = (z/\delta) + (1/24)(a/\delta)^2[6\tanh(z/\delta) - z/\delta]$ leading to the confining potential $\tilde{V}(\xi) = -2\mathrm{sech}^2[y(\xi)]$ with $y(\xi) = \xi + (1/24)(a/\delta)^2(6\tanh\xi - \xi)$. According to Thacker *et al.* [39], a reflectionless potential with two bound states must obey Eq. (8). However, the confining potential induced by a narrow DW as derived above cannot be described by a four-parameter reflectionless potential Eq. (8), and indeed necessarily induces reflections. An expansion up to higher order will not change this conclusion. Therefore, the SW cannot be totally transmitted anymore, confirming the numerical results.

The k-dependent SW transmissions for different parameters D/J are shown in Fig. 3(b), where the k values are obtained by fast Fourier transformation of the computed SW mode amplitudes [25]. The wave vectors k of interest range here from zero up to $0.8\pi/a$, corresponding to a very short wavelength ($2.5a$) beyond which a classical spin model might become unreliable [41]. In agreement with previous results, there is no detectable reflection in the calculations with $D/J < 0.01$. However, for a large anisotropy, the SW will be only partially transmitted through the DW, with transmission probability monotonically decreasing with increasing wave vector k. These results are very different from those obtained with a local spin-spiral approximation, i.e., a constant pitch within the DW width [42], which leads to perfect transmission for SWs with large k but hindered propagation at long wavelengths [20]. This artifact is caused by the unphysical kinks in the magnetization texture of the spin-spiral model. We also have a message for micromagnetic simulations in which the continuum Hamiltonian $\mathcal{H} = J'(\partial\mathbf{m}/\partial z)^2/2 - Dm_z^2$ is discretized into block spins $J'\partial^2\mathbf{m}_n/\partial z^2 = J'(\mathbf{m}_{n-1} - 2\mathbf{m}_n + \mathbf{m}_{n+1})/(\Delta z)^2$. The mesh size Δz is found here to be critical, since SW reflections that are artifacts in a continuum model occur unless $\pi\sqrt{J'/2D} \geq 22\Delta z$.

Our results should be relevant for systems with close to atomically sharp DWs such as YIG thin films. In the case of a narrow atomic-scale DW, SWs are reflected, which modifies the heat transport as $\dot{Q}_{\mathrm{DW}} = \dot{Q} + \Delta\dot{Q}_{\mathrm{DW}}$, where

$$\Delta\dot{Q}_{\mathrm{DW}} = \frac{\Delta T}{2\pi}\int d\omega(|t_\omega|^2 - 1)\hbar\omega\frac{\partial n_B(\omega, T)}{\partial T}. \tag{9}$$

Since $\Delta\dot{Q}_{\mathrm{DW}} < 0$, the DW decreases the heat conductance. We can estimate the reduction of the heat current by SW reflection at low temperatures where magnons exist only at the bottom of SW band ($k = 0$) and $|t(k = 0)|^2$ can be used to estimate the total transmission probability such that $\Delta\dot{Q}_{\mathrm{DW}}/\dot{Q} \approx |t(k = 0)|^2 - 1$. When $D/J = 0.4$, $\Delta\dot{Q}_{\mathrm{DW}}/\dot{Q} \sim -35\%$. At room temperature, k_BT is larger than the exchange energy $J \approx 40$ K in YIG [22,26] and magnons with large wave numbers become important for the heat transport. The spin wave reflection becomes significant when $\delta \lesssim (10/\pi)a$, where $a = 1.24$ nm in YIG [19,22,26]. However, at room temperature a multisublattice model should be used for YIG, leading to multiple bands and complex SW transport properties [26], which is beyond the scope of this work.

Ultranarrow DWs are sensitive to crystal lattice pinning: the A- and B-type walls in the 1D model (Fig. 1) have different ground-state energies [18]. In such a "Peierls" potential, a DW has to overcome an energy barrier when moving from one atomic plane to another and a threshold external force is necessary to assist the DW motion [18]. Novoselov *et al.* [19] indeed observed a critical magnetic field for field-driven atomic-scale DW dynamics. Consequently, to propagate DWs even in perfect wires, an intrinsic critical heat/spin current exists. According to Ref. [14], a temperature gradient of 1 K/nm creates a pressure corresponding to a field $H = 5$ mT for a magnetic insulator with a saturation magnetization $M_s = 2 \times 10^6$ A/m. We estimate the critical temperature gradient to overcome the atomic pinning as 0.1 K/μm for the critical magnetic field value $H_c = 0.7$ G and $M_s = 1.6 \times 10^4$ A/m reported in Ref. [19].

In conclusion, we studied the heat transport by SWs through magnetic DWs. When the DW width becomes of the order of a few lattice constants, a second bound state emerges that is absent in the continuum approximation and causes strong SW reflection and a significant DW heat conductance. Our results are relevant for ultrahigh-density DW-based storage devices [43] made from insulating ferromagnets. The generalization of the present model to higher dimensions in which dipolar interactions become important as well as to antiferromagnets and multiferroic nanostructures with strong uniaxial anisotropies should be the subject of future research.

We thank Xiang Rong Wang and Akashdeep Kamra for helpful discussions. This work is supported by the FOM foundation, DFG Priority Program 1538 SpinCat, and EG-STREP MACALO.

[1] V. V. Kruglyak, S. O. Demokritov, and D. Grundler, J. Phys. D **43**, 260301 (2010); B. Lenk, H. Ulrichs, F. Garbs, and M. Münzenberg, Phys. Rep. **507**, 107 (2011).

[2] T. Schneider, A. A. Serga, B. Leven, B. Hillebrands, R. L. Stamps, and M. P. Kostylev, Appl. Phys. Lett. **92**, 022505 (2008).

[3] A. Khitun, M. Q. Bao, and K. L. Wang, IEEE Trans. Magn. **44**, 2141 (2008).

[4] V. Vlaminck and M. Bailleul, Science **322**, 410 (2008).

[5] K. Sekiguchi, K. Yamada, S. M. Seo, K. J. Lee, D. Chiba, K. Kobayashi, and T. Ono, Phys. Rev. Lett. **108**, 017203 (2012).

[6] S. S. P. Parkin, M. Hayashi, and L. Thomas, Science **320**, 190 (2008).

[7] D. A. Allwood, G. Xiong, C. C. Faulkner, D. Atkinson, D. Petit, and R. P. Cowburn, Science **309**, 1688 (2005).

[8] R. Hertel, W. Wulfhekel, and J. Kirschner, Phys. Rev. Lett. **93**, 257202 (2004).

[9] C. Bayer, H. Schultheiss, B. Hillebrands, and R. L. Stamps, IEEE Trans. Magn. **41**, 3094 (2005).

[10] S. J. Hermsdoerfer, H. Schultheiss, C. Rausch, S. Schäfer, B. Leven, S. K. Kim, and B. Hillebrands, Appl. Phys. Lett. **94**, 223510 (2009).

[11] A. V. Mikhaĭlov and A. I. Yaremchuk, Pis'ma Zh. Eksp. Teor. Fiz. **39**, 296 (1984); [JETP Lett. **39**, 354 (1984)].

[12] D. S. Han, S. K. Kim, J. Y. Lee, S. J. Hermsdoerfer, H. Schultheiss, B. Leven, and B. Hillebrands, Appl. Phys. Lett. **94**, 112502 (2009).

[13] M. Jamali, H. Yang, and K. J. Lee, Appl. Phys. Lett. **96**, 242501 (2010).

[14] D. Hinzke and U. Nowak, Phys. Rev. Lett. **107**, 027205 (2011).

[15] P. Yan, X. S. Wang, and X. R. Wang, Phys. Rev. Lett. **107**, 177207 (2011).

[16] A. A. Kovalev and Y. Tserkovnyak, Europhys. Lett. **97**, 67002 (2012).

[17] C. A. Jenkins and D. I. Paul, J. Appl. Phys. **111**, 013915 (2012).

[18] H. R. Hilzinger and H. Kronmüller, Phys. Status Solidi **54**, 593 (1972).

[19] K. S. Novoselov, A. K. Geim, S. V. Dubonos, E. W. Hill, and I. V. Grigorieva, Nature (London) **426**, 812 (2003).

[20] S. H. Liu, J. Magn. Magn. Mater. **12**, 262 (1979).

[21] M. Hatami, G. E. W. Bauer, Q. Zhang, and P. J. Kelly, Phys. Rev. Lett. **99**, 066603 (2007).

[22] I. S. Tupitsyn, P. C. E. Stamp, and A. L. Burin, Phys. Rev. Lett. **100**, 257202 (2008); A. Kreisel, F. Sauli, L. Bartosch, and P. Kopietz, Eur. Phys. J. B **71**, 59 (2009).

[23] R. Wieser, U. Nowak, and K. D. Usadel, Phys. Rev. B **69**, 064401 (2004).

[24] A. V. Ferrer, P. F. Farinas, and A. O. Caldeira, Phys. Rev. Lett. **91**, 226803 (2003).

[25] R. Wieser, E. Y. Vedmedenko, and R. Wiesendanger, Phys. Rev. B **81**, 024405 (2010).

[26] V. Cherepanov, I. Kolokolov, and V. L'vov, Phys. Rep. **229**, 81 (1993).

[27] J. E. Rives, G. S. Dixon, and D. Walton, J. Appl. Phys. **40**, 1555 (1969).

[28] R. L. Douglass, Phys. Rev. **129**, 1132 (1963).

[29] F. Meier and D. Loss, Phys. Rev. Lett. **90**, 167204 (2003).

[30] E. E. Fullerton, J. S. Jiang, M. Grimsditch, C. H. Sowers, and S. D. Bader, Phys. Rev. B **58**, 12193 (1998).

[31] N. L. Schryer and L. R. Walker, J. Appl. Phys. **45**, 5406 (1974).

[32] G. Tatara and H. Fukuyama, Phys. Rev. Lett. **72**, 772 (1994).

[33] V. K. Dugaev, P. Bruno, B. Canals, and C. Lacroix, Phys. Rev. B **72**, 024456 (2005); K. Y. Guslienko, G. R. Aranda, and J. M. Gonzalez, Phys. Rev. B **81**, 014414 (2010).

[34] A. Brataas, G. Tatara, and G. E. W. Bauer, Phys. Rev. B **60**, 3406 (1999).

[35] R. Wieser, E. Y. Vedmedenko, and R. Wiesendanger, Phys. Rev. B **79**, 144412 (2009).

[36] T. Koma and M. Yamanaka, Phys. Rev. B **65**, 104434 (2002).

[37] B. Barbara, J. Magn. Magn. Mater. **129**, 79 (1994).

[38] A. Vindigni, Inorg. Chim. Acta **361**, 3731 (2008).

[39] H. B. Thacker, C. Quigg, and J. L. Rosner, Phys. Rev. D **18**, 274 (1978).

[40] K. M. Case and M. Kac, J. Math. Phys. (N.Y.) **14**, 594 (1973); K. M. Case, J. Math. Phys. (N.Y.) **14**, 916 (1973).

[41] J. Prokop, W. X. Tang, Y. Zhang, I. Tudosa, T. R. F. Peixoto, Kh. Zakeri, and J. Kirschner, Phys. Rev. Lett. **102**, 177206 (2009).

[42] R. P. van Gorkom, A. Brataas, and G. E. W. Bauer, Phys. Rev. Lett. **83**, 4401 (1999).

[43] R. Nebashi, N. Sakimura, Y. Tsuji, S. Fukami, H. Honjo, S. Saito, S. Miura, N. Ishiwata, K. Kinoshita, T. Hanyu, T. Endoh, N. Kasai, H. Ohno, and T. Sugibayashi, IEEE Symp. VLSI Circuit Dig. Tech. Pap. 300 (2011).